© IWA Publishing 2020
632

Water Practice & Technology Vol 15 No 3
doi: 10.2166/wpt.2020.049

Change dynamics of land-use and land-cover for tropical wetland management

N. López, A. Márquez Romance* and E. Guevara Pérez

Environmental and Hydrological Research Center, University of Carabobo, Naguanagua, Venezuela

*Corresponding author. E-mail: ammarquez@uc.edu.ve

Abstract

In hydrographic basins with wetlands, changes in land use (LU) and land cover (LC) impact the conservation of natural resources, leading to dynamics analysis for integral management. A method is proposed offering greater accuracy in determining the LU and LC bi-temporal and spatial change dynamics in tropical wetlands. LU and LC monitoring is based on Landsat images from 1986 to 2017. 'Pre-classification' and 'post-classification' methods are applied. In the former, reflectance image differencing and principal component N° 1 image differencing are analyzed to estimate the rate of change/no change area. In the latter, supervised classification is carried out of image pairs from different dates. The principal components method shows that principal component N° 1 collects between 88 and 93% of the reflectance variance in *n* spectral bands of each satellite image, which improves accuracy in determining LU and LC change dynamics.

Key words: changes, cover, dynamics, images, multi-temporal

Highlights

- Land use and land cover change detection techniques.
- Change detection techniques applied to wetlands.
- Satellite image classification techniques.
- Digital image classification techniques applied to tropical wetlands.
- Comparison of change detection techniques.

INTRODUCTION

Sustainable use and management of tropical coastal wetlands requires assessment of direct and indirect human impact on these ecosystems. Humans exert pressure on vegetation and agricultural land in wetland areas, turning to agriculture as a sustainable resource for the population. The ecosystem's resilience and recovery capacity must be determined after such impacts. They are often found in sensitive areas that are hard to reach due to the existence of habitats that provide shelter, flooded conditions and thick vegetation. Thus, remote sensing and geographical information systems (GIS) are useful tools for monitoring the spatial and temporal tendencies of land-use and land-cover (LULC) dynamics in tropical basin wetlands (Dahdouh-Guebas 2002). An assessment of the displacement of the island's estuary coast and sand barrier along the Virginia, Maryland, and New Jersey coasts, using GIS techniques, documented the impacts of Hurricane Sandy such as long-term changes, which include the impacts of past storms (Plant *et al.* 2018).

Different change detection techniques based on pixels – the basic image analysis unit – are classified as: (i) pre-classification for measuring change/no change: image differencing, image ratioing,

Water Practice & Technology Vol 15 No 3
doi: 10.2166/wpt.2020.049

regression analysis, vegetation index differencing, normalized differencing vegetation index (NDVI), change vector analysis (CVA), and principal component analysis (PCA); (ii) comparison based on classification for measuring detailed change (post-classification and multi-temporal direct or compound classification) (Hussain *et al.* 2013).

To assess wetland change in Kafue Flats, Zambia, Munyati (2000) used Landsat MSS images and Thematic Mapper™, as well as the change detection technique based on post-classification comparison, carrying out a supervised classification using a maximum likelihood algorithm. This methodology seems to be applicable for monitoring continental wetland systems in southern Africa.

According to Hayes & Sader (2001), the Guatemalan Mayan Biosphere Reservoir has experienced high rates of deforestation corresponding to human migration and agricultural frontier expansion. Techniques for detecting change with multi-temporal Landsat TM satellite images were used. Three pre-classification methods were assessed: (i) NDVI image differencing, (ii) principal component image differencing and (iii) RGB-NDVI change detection; NDVI values NDV(j) = (TM4 – TM3)/(TM4 + TM3) from three dates were assigned the colors red, green and blue, and categorized high, medium or low. The highest accuracy was accomplished by the RGB-NDVI method (85%).

In the Bharthapuzha River Basin, India, LULC changes were analyzed using Landsat™ multispectral images. The change detection technique was post-classification comparison using a supervised classification algorithm. An 8.7% depletion of the wetland's agricultural area was observed, and urban expansion in the basin increased by 32%. The study highlights the need for a scientific management plan for river basin sustainability (Nikhil & Azeez 2010).

For seasonal variations of the Malinda wetland, Tanzania, Kuria *et al.* (2014) used orthophotos from unmanned aerial vehicle (UAV) images fused with Spotlight TerraSAR-X dual-polarized radar data, combining two techniques for change detection: image differencing based on unsupervised classification by applying maximum likelihood diffuse inference and change vector analysis (CVA). The accuracy of determination of land covers was satisfactory.

Mwita (2016) assessed restoration of the Usangu wetland, Tanzania, using Landsat time-series images, and the NDVI change detection method of image differencing. The land cover and swamp size results show a need to implement measures for wetland protection and sustainability.

For the Surjpur wetland, Uttar Pradesh, India, Saha *et al.* (2017) studied LULC changes as a component of human interactions with the environment, using Landsat 7 and Landsat 8 OLI images, and comparing them with Google Earth images. LULC changes were detected by post-classification comparison. Saha *et al.* recommend wetland management and restoration.

Spruce *et al.* (2020) conducted a LULC mapping study for the Lower Mekong Basin, Asia, using GIS along with LULC change maps from 1997 to 2010 to be used as inputs to the SWAT hydrological model. The main purpose was the evaluation of the results and support for the management and planning of water and terrestrial resources.

The purpose of this study was to analyze the dynamics of bi-temporal and spatial changes in land use (LU) and land cover (LC) in a tropical basin with a natural wetland – the Urama River, Venezuela. The wetland has been impacted because of land demand for agricultural and livestock production (Petrochemistry of Venezuela (PEQUIVEN) 2014). The study was carried out using time periods 1986–1991, 2000–2008, and 2015–2017. The methodology included digital preprocessing of Landsat MSS, TM, ETM+ and OLI images to generate classification maps LU and LC type, by applying pre- and post- classification techniques. This novel method enables greater accuracy in determining the dynamics of LU and LC bi-temporal and spatial changes in tropical wetlands, thus contributing to their management. The change/no change of cover use is determined by the qualitative pre-classification technique, and bi-temporal change variation by classes is determined by the quantitative post-classification techniques, and thus the magnitude and direction. This enables definition of the proportionality of dynamic factors for management models for wetlands in tropical basins.

Water Practice & Technology Vol 15 No 3
doi: 10.2166/wpt.2020.049

STUDY AREA

The study area is in the central North Coastal Region, Venezuela, whose boundaries are between the Carabobo and Yaracuy states. There are two rivers, the Temerla and Canoabo, in the Urama Basin. On the alluvial plain, a natural wetland is created by discharge to the Caribbean (Figure 1).

MATERIALS AND METHODS

Phase 1. Satellite image data collection and references

Seven multispectral images acquired by Landsat sensors were used as data sources in this study. They are available on the Earth Explorer website (USGS 2017). The criterion used to analyze LULC change detection was the 31-year data collection period from 1986 to 2017, including 1991, 2000, 2008, 2015, 2016 to 2017 (Table 1).

Phase 2. Preliminary satellite image processing

Preliminary Landsat image processing comprised making absolute and relative geometric, radiometric, topographic and atmospheric corrections corresponding to each image (Jensen 2009).

Phase 3: application of change detection methods

The selected methods are: (1) pre-classification: (A) algebraic methods (reflectance image differencing) and (B) transformation method (principal components image differencing); (2) post-classification method. The procedures are as follows.

Pre-classification method based on reflectance image differencing

Two multi-temporal images co-registered accurately are used corresponding to times t_1 and t_2. A pixel by pixel difference operation is applied to produce a residual image representing the change between t_1 and t_2 (Singh 1989; Hussain *et al.* 2013).

Pre-classification method based on principal component image differencing

This involves a linear transformation of variables corresponding to rotation and translation of the original coordinate system (Singh 1989; Marquez *et al.* 2019), to reduce the dimensionality of the reflectance variable in the spectral bands to one or two components before applying the LULC change detection techniques.

Post-classification method

Change dynamics is estimated as the attribute difference between the initial and final years (Jensen 2009), and the supervised classification technique is used (Marquez *et al.* 2019). Once classified, the map is analyzed to elaborate the recoded version by comparing the reference image from websites like Google Earth corresponding to each time period studied, in conjunction with field reconnaissance, which enables identification of spectrally homogeneous classes (PEQUIVEN 2014; Marquez *et al.* 2018a, 2018b).

Water Practice & Technology Vol 15 No 3
doi: 10.2166/wpt.2020.049

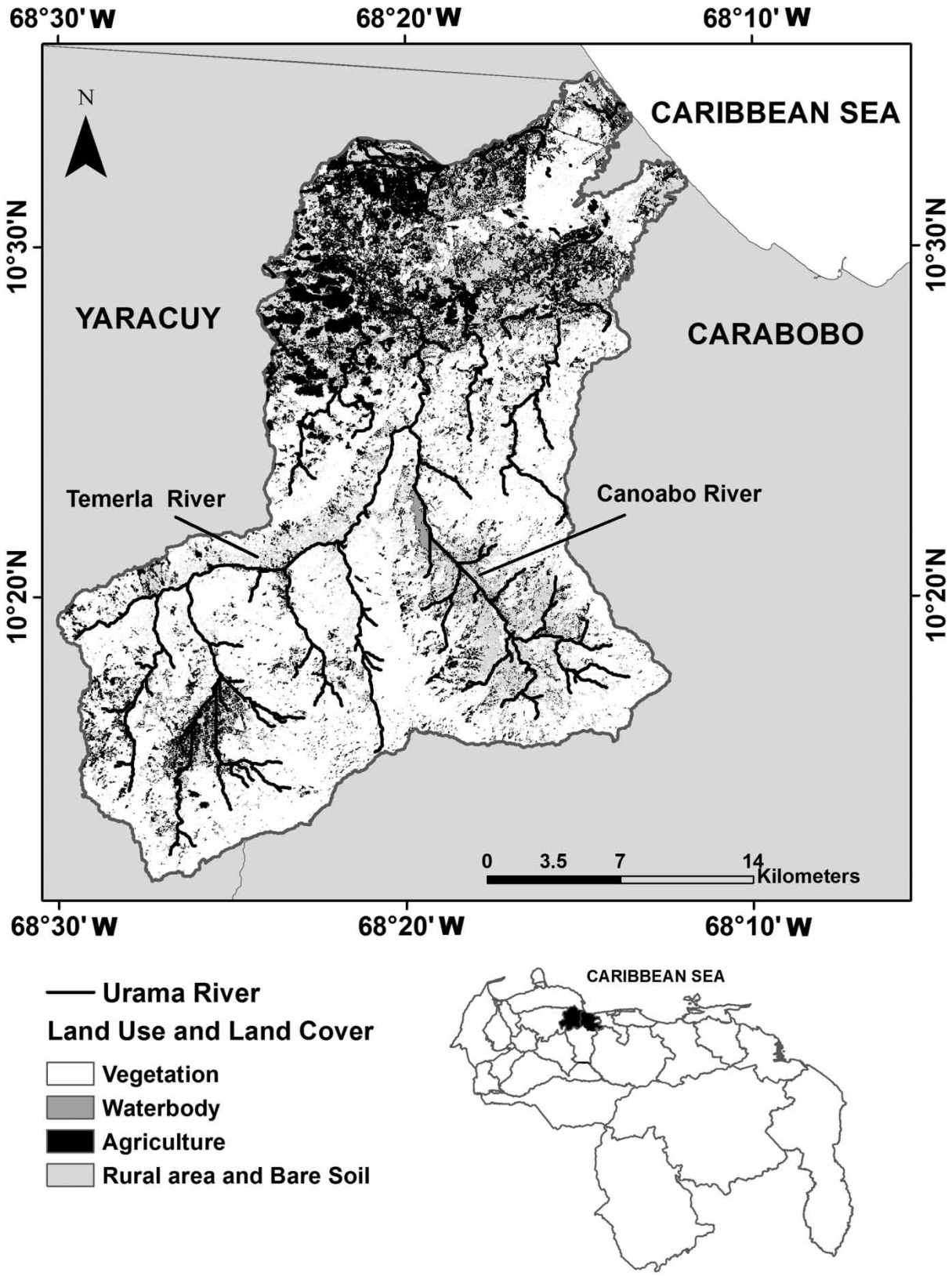

Figure 1 | Urama Basin, Venezuela. LULC were derived from a Landsat 7 ETM image acquired on January 14, 2000 (source U.S. Geological Survey). The river was generated using Dataset: ASF DAAC (2015), ALOS PALSAR_Radiometric_Terrain_Corrected_-high_res (Data source JAXA/METI 2007). Accessed through ASF DAAC on 20 May 2020. DOI: 10.5067/Z97HFCNKR6VA.

Table 1 | Landsat image characteristics

Year	Scene identification	Date	Sensor	N° of bands	Azimuth solar angle	Solar elevation angle	Zenith angle
1986	LM50050531986239AAA05	27/8/1986	LANDSAT_5 'MSS'	4	86.91	55.01	35.00
1991	LM50050531991157AAA03	6/6/1991	LANDSAT_5 'MSS'	4	64.85	54.76	35.23
2000	LE70050532000014SGS01	14/1/2000	LANDSAT_7 'ETM'	8	137.52	47.22	42.77
2008	LT50050532008156CHM00	4/6/2008	LANDSAT_5 'TM'	7	61.71	60.42	29.58
2015	LC80050532015271LGN01	28/9/2015	LANDSAT_8'OLI_TIRS'	9	116.64	63.96	26.03
2016	LC80050532016066LGN01	6/3/2016	LANDSAT_8'OLI_TIRS'	9	117.54	57.89	32.11
2017	LC80050532017276LGN00	3/10/2017	LANDSAT_8'OLI_TIRS'	11	121.36	63.31	26.69

Map projection parameters (USGS): (a) UTM Projection, (b) WGS1984 Datum, (c) WGS84 Ellipsoid, (d) UTM Zone 19 N, (e) cubic convolution.
Source: Data from the Earth Explorer (USGS 2017).

Water Practice & Technology Vol 15 No 3
doi: 10.2166/wpt.2020.049

Water Practice & Technology Vol 15 No 3
doi: 10.2166/wpt.2020.049

RESULTS AND DISCUSSION

Pre-classification reflectance image differencing method

The results are expressed by interval limits for the pixel distribution of change/no change areas in the river basin for the period 1986–2017. The limit criterion for change/no change areas is based on an interval defined by the mean *(μ)* +/− *n* standard deviation *(σ)*, assuming that the distribution of the reflectance differencing image pixels in the near-infrared spectral region (NIR) approaches a normal distribution function and that the change/no change area limits are equidistant from the mean. The first limit is no change area equal to the mean *(μ)* +/− *1* standard deviation *(σ)*. The second is equal to the change area obtained as $<\mu-1\sigma,>\mu+1\sigma$; respectively; giving the lower limit (LL) and upper limit (UL).

Bi-temporal image differencing shows a slight tendency towards symmetry with respect to the mean *(μ)* for the time periods 1986–2017, 2000–2017, 2008–2017, 2015–2017 and 2016–2017. A bias or asymmetry was found for the period 1991–2017 (Table 2). The standard deviation is in the order of 10^1–10^2.

Table 2 | Bi-temporal reflectance image differencing results for change/no change areas in the Urama Basin from 1986 to 2017

Bi-temporal images	1986–2017	1991–2017	2000–2017	2008–2017	2015–2017	2016–2017
μ	2.68	11.17	(−3.27)	(−0.23)	(−3.08)	(−3.07)
Σ	10.39	11.47	9.41	8.08	12.08	8.51
LL: < μ – 1σ	−75- −14	−76- −14	−90- −16	−86- −17	−88- −7	−85- −11
NC: μ +/− 1σ	−14– 13	−14 - 34	−16 - 8	−17 - 22	−7 - 12	−11 - 9
UL: > μ +1σ	13 – 87	34 - 88	9-74	22 - 74	12 - 88	9 - 55

Parameters: mean: μ, standard deviation: σ, no change NC: μ +/− 1σ lower limit (LL): <μ–1σ, upper limit (UL): >μ + 1σ.

Three categories are defined for the results of the bi-temporal reflectance image differencing as expressed by the error matrix (Table 3) in the change detection accuracy for the images observed: decrease (DEC), no change (NC), and increase (INC). The reflectance differencing image pixels associated with reflectance DEC are negative because the NIR reflectance observed in the image year for time t_2 is less than the NIR reflectance observed for t_1. The NC pixels are taken from the limit mean region +/− 1 standard deviation centered at zero, whose value shows that the image reflectances at t_1 are equal to those at t_2. The INC image pixels are those where the reflectance difference is greater for the reflectance image for t_2 than the observed reflectance differencing image (ORDI) for t_1. Thus, for the period 2016–2017: (1) DEC in the predicted reflectance differencing image (PRDI)

Table 3 | Bi-temporal reflectance image differencing results – error matrix of change detection accuracy in the Urama Basin, 2016–2017

		ORDI, 2016–2017					
		DEC	NC	INC	Row total	User accuracy (%)	K
PRDI	DEC	109	32	0	141	77	0.71
	NC	0	33	0	33	100	1.00
	INC	0	32	94	126	75	0.60
	Column total	109	97	94	300		
	Producer accuracy (%)	100	34	100			
Total accuracy (%)							79
Kappa statistic							0.77

Water Practice & Technology Vol 15 No 3
doi: 10.2166/wpt.2020.049

corresponding to DEC in ORDI: 109, NC in ORDI: 32, INC in ORDI: 0. The accuracy and Kappa indices in the error matrix are 79% and 0.77, respectively.

Comparison of PRDI with ORDI shows that 236 out of 300 pixels match, justifying the 79% accuracy obtained. The differences between predicted and observed pixels are based on the change/no change interval selection criterion, which depends on the number of times assigned to the standard deviation, defined by the change/no change threshold. For example, the NC pixels selected in the PRDI showed a user accuracy of 100% in the ORDI, for a sample of 31 randomly distributed points and $K = 1$, while, in the pixels where change occurred – increase or decrease – user accuracy varied between 75 and 77%, and K between 0.6 and 0.71 (Table 3). The Kappa statistic takes into account the non-diagonal elements by comparing them with the total accuracy index. Sinha & Kumar (2013) put forward a two-step thresholding approach for threshold value determination for the spectrally increased and decreased area using NDVI differencing image.

The results show that there is no significant difference in accuracy when distribution is nearly symmetric, confirming the importance of considering normal data distribution in LC change/no change analysis. Accuracies exceeding 90% and K 0.89 were achieved from all the change/no change determination methods used. Comparison with the accuracies in this study has shown that there are no significant differences between the accuracy and Kappa indices for the reflectance differencing image.

The reflectance differencing images during the six periods – 1986–2017, 1991–2017, 2000–2017, 2008–2017, 2015–2017, 2016–2017 – show the occurrence of positive, negative and no change values (Figure 2). The changes occur mainly during the longer periods 1986–2017 and 1991–2017. Most of the Urama Basin is covered by vegetation. Reflectance decrease (white dots in Figure 1) could be due to change from vegetation to degraded soil. Reflectance increase (black) could arise from a change to agricultural use.

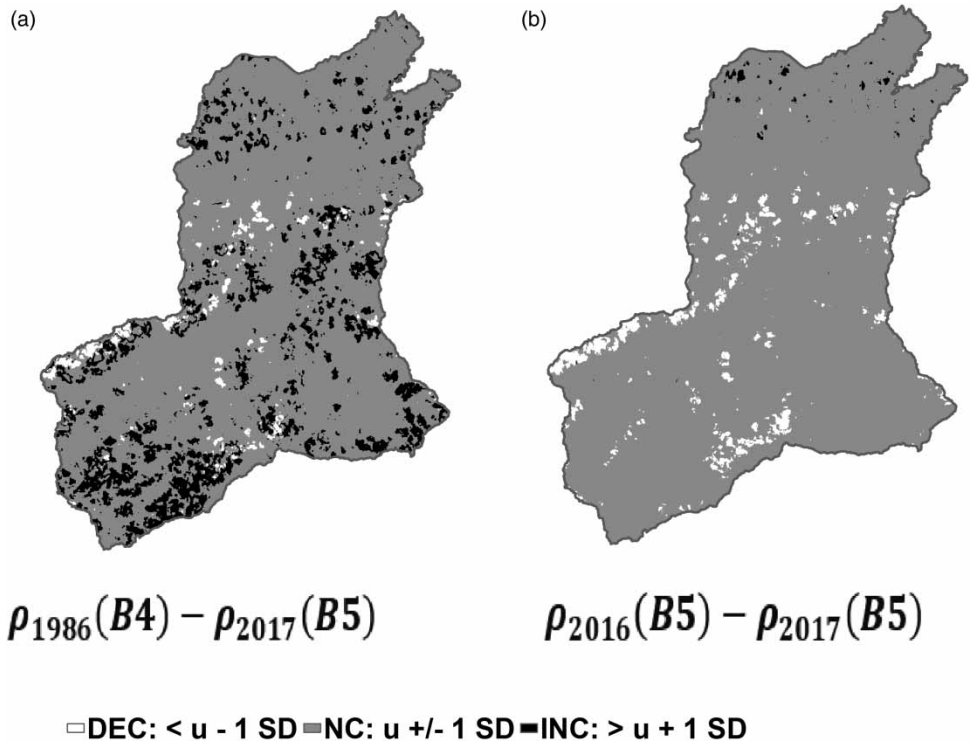

Figure 2 | Reflectance image differencing results in the Urama Basin – 1986–2017: Spectral band 4 (B4) selected from Landsat 5TM (1986, 1991, 2008) and Landsat 7 ETM (2000) reflectance images; Spectral band 5 (B5) for Landsat 8 OLI (2015, 2016 and 2017) reflectance images. Legend: White (DEC), Black (INC), Gray (NC).

Water Practice & Technology Vol 15 No 3
doi: 10.2166/wpt.2020.049

Pre-classification method results – principal component image differencing

The pre-classification method results based on principal component (PC) image differencing are derived by transforming the reflectance variables (ρ) in the principal component for each Landsat image. The Landsat 8 OLI image transformation for 2017 is shown in Table 4, for example, and the subsequent PC1 differences in Tables 4 and 5. The correlated reflectance dataset contained in the seven 2017 Landsat image spectral bands is transformed into a dataset consisting of variables identified as PCs, which are uncorrelated linear combinations of the original variables represented by the reflectances in the seven spectral bands.

Table 4 | PC transformation results expressed by reflectance image covariance matrix and correlation matrix (%) 2017 in the Urama Basin

Landsat spectral band	PC1	PC2	PC3	PC4	PC5	PC6	PC7
Reflectance image covariance matrix (%) 2017							
B1	33.96	32.68	35.15	33.78	68.67	48.02	31.62
B2	32.68	31.59	33.92	32.68	65.55	46.25	30.56
B3	35.15	33.92	37.99	35.90	85.71	57.12	35.77
B4	33.78	32.68	35.90	34.61	73.45	51.62	33.43
B5	68.67	65.55	85.71	73.45	325.28	179.80	93.96
B6	48.02	46.25	57.12	51.62	179.80	109.21	61.18
B7	31.62	30.56	35.77	33.43	93.96	61.18	36.77
Reflectance image correlation matrix 2017							
B1	1.00	0.99	0.97	0.98	0.65	0.78	0.89
B2	0.99	1.00	0.97	0.98	0.64	0.78	0.89
B3	0.97	0.97	1.00	0.98	0.77	0.88	0.95
B4	0.98	0.98	0.98	1.00	0.69	0.83	0.93
B5	0.65	0.64	0.77	0.69	1.00	0.95	0.85
B6	0.78	0.78	0.88	0.83	0.95	1.00	0.96
B7	0.89	0.89	0.95	0.93	0.85	0.96	1.00

Table 5 | PC transformation results expressed by reflectance image eigenvalues from 1986 to 2017 in the Urama Basin

	PC	PC1	PC2	PC3	PC4	PC5	PC6	PC7
1986	Eigenvalues	767.51	86.34	10.42	0.49			
	Proportion	88.75	9.98	1.20	0.057			
1991	Eigenvalues	955.49	78.67	8.32	1.00			
	Proportion	91.56	7.53	0.79	0.096			
2000	Eigenvalues	1118.67	106.68	12.67	3.57	0.488	0.21	0.14
	Proportion	90.03	8.58	1.02	0.29	0.039	0.016	0.011
2008	Eigenvalues	3553.35	743.80	28.87	14.87	3.916	1.329	0.387
	Proportion	81.75	17.11	0.66	0.34	0.09	0.030	0.008
2015	Eigenvalues	496.94	73.39	11.85	0.38	0.27	0.114	0.068
	Proportion	85.233	12.58	2.033	0.064	0.047	0.019	0.011
2016	Eigenvalues	395.01	20.138	6.197	0.722	0.330	0.178	0.104
	Proportion	93.453	4.764	1.466	0.171	0.078	0.042	0.024
2017	Eigenvalues	544.938	59.492	438.460	0.257	0.216	0.087	0.059
	Proportion	89.41	9.76	0.72	0.042	0.035	0.014	0.0097

Water Practice & Technology Vol 15 No 3
doi: 10.2166/wpt.2020.049

For example, the PC N° 1 (PC1) can be expressed mathematically as the orthogonal linear combination (Equation (1)):

$$PC_1 = 33.96\rho_{b1} + 32.68\rho_{b2} + 35.15\rho_{b3} + 33.78\rho_{b4} + 68.87\rho_{b5} + 48.02\rho_{b6} + 31.62\rho_{b7}. \quad (1)$$

As observed in Equation (1), the reflectance variable coefficients (covariances) are similar in the first four bands, where reflectances have been detected by sensors in the optical region. This is confirmed as the reflectance dataset correlation coefficients are not statistically different between the PCs PC1 to PC4 (Table 4), but differ slightly in the others (PC5 to PC7).

The similarity in the reflectance covariance coefficients in the optical region bands, and the difference with respect to band 5 (NIR) covariance might arise because the predominant landscape cover is vegetation and relates to the spectral response from this type of cover. The spectral reflectance profile obtained from the type of vegetation found in the Urama Basin is associated with slight and mild reflectance variations in the optical region, ranging from 5 to 7%. In the NIR, reflectance increases from 5 (optical region) to 30%. According to Jensen (2009), healthy green leaves absorb radiant energy in the blue and red portions of the spectrum where incident light is required for photosynthesis. In the NIR, healthy green vegetation is generally characterized by high reflectance (40–60%), high transmittance (40–60%) through the leaf to its underside, and relatively low absorption (5–10%).

The PC transformation results are also expressed by reflectance image eigenvalues from 1986 to 2017. Thus, the variance vector of the PCs or eigenvalues in the Landsat 8 OLI image from 10/03/2017 is: Var $[\rho(PC_{1-7})] = (544.938, 59.492, 4.384, 0.257, 0.216, 0.087, 0.059)$; while the population variance is represented by the sum of eigenvalues = 604.43 (Table 5). The highest proportion of the total population variance is represented by PC1, varying between 81.75 and 93.45% for images from 1986 to 2017 (Table 5). The PC1 selection criterion as the image to be included in the change detection technique based on principal component image differencing is that the first PC expresses the maximum possible proportion of variance in the original dataset (Ingebritsen & Lyon 1985).

The PC1 differencing images covering 1986–2017 and 2016–2017 are shown in Figure 3. The changes are shown as in Figure 2. Most changes are associated with reflectance increases through

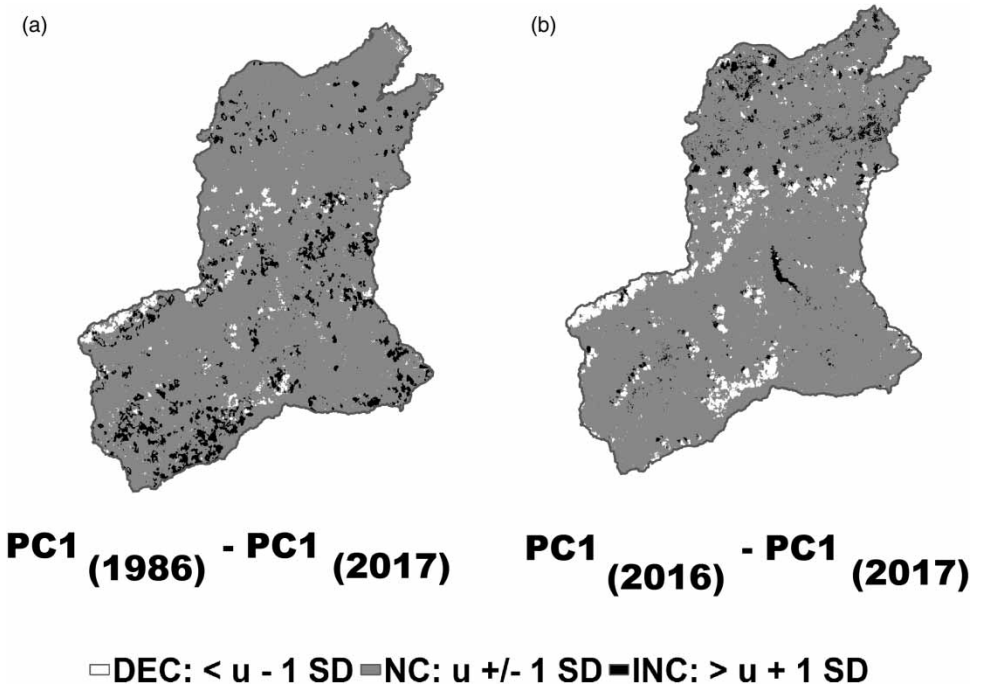

Figure 3 | PC reflectance differencing results in the Urama Basin from 1986 to 2017. Legend: White spot (DEC); Black (INC); Gray (NC).

Water Practice & Technology Vol 15 No 3
doi: 10.2166/wpt.2020.049

time. Like the reflectance differencing image method, the principal change could be replacement of the vegetation by agricultural use (Hayes & Sader 2001).This method highlights the reflectance increase in the reservoir in the middle of the river basin from 2000 to 2017, in particular. This could be due to a change from clear water to sediment and algae caused by eutrophication. As the concentration of suspended sediments and algae-laden increase in clear water, reflectance increases in all wavelengths for both clayey and silty soils (Han & Rundquist 1997; Lodhi *et al.* 1997).

Post-classification method results

The post-classification method results include procuring the statistics associated with two stages: (1) generation of the LULC classification map based on reflectance images and (2) recoding the classified map based on the acquired reference image from Google Earth.

The post-classification comparison method results using the image classification error matrix for 1986 are shown in Table 6. Some 12,637 randomly selected pixels on the classified map (CM), (left column), were compared with the uses observed in the 2017 Google Earth reference image (RI) (top row). The classes are: 1. Vegetation (C1), 2. Waterbody (C2), 3. Agriculture (C3), 4. Rural area (C4), 5. Bare soil (C5), 6. Clouds (C6), and 7. Shadows (C7).

Table 6 | Post-classification comparison method results

		Reference data									
		Google Earth Reference Image (RI)									
	UT-CT	**C1**	**C2**	**C3**	**C4**	**C5**	**C6**	**C7**	**Row total**	**User accuracy (%)**	**Kappa index**
1986 Classified Map (CM)	C1	**8,411**		8					8,419	99.90	
	C2		**623**						623	100	
	C3	133		**775**		2			910	85.16	
	C4	200		9	**34**				243	13.99	
	C5	7	1			**446**	2	2	458	97.38	
	C6					3	**1,513**		1,516	99.80	
	C7		12					**456**	468	97.44	
Column total		8,751	636	792	4	451	1,515	458	**12,637**		
Producer accuracy (%)		96.11	97.96	97.85	100	98.89	99.87	99.56			
Global accuracy (%)										**97.00**	
Kappa index											**0.942**

Error matrix corresponding to LULC classification maps based on reflectance images in the Urama Basin for 1986.

As for the 1986 Urama Basin classified map (Table 6), vegetation (C1) was associated with 8,419 pixels, of which 8,411 coincided with C1 in RI and 8 corresponded to agriculture (C3) in RI, resulting in 99.9% user accuracy. In the waterbody (C2): 623 pixels corresponded exactly with C2 in RI –user accuracy 100%. For agriculture (C3): of 910 pixels, 133 corresponded to vegetation (C1) in RI, 775 with agriculture class (C3) and 2 with bare soil (C5). Accuracy was thus 97% and $K = 0.942$.

The four post-classification method accuracy indices can be interpreted in the seven classified maps using statistics for a sample size equal to 12,637 pixels (Table 6, 1986 image): interval (I), mean (M) and standard deviation (SD): (1) accuracy of change/no change detection: I: 72 and 99%; M: 94.11% and SD: 9.81%. (2) Kappa Coefficient: I: 0.51 and 0.99; M: 0.89 and SD: 0.17. Trodd (1995) reviewed the methods used to assess image classifications in a literature survey of 84 classifications reported in 25 papers published in major journals from 1994 to 1995; finding that the mean accuracy was 67.66%. Foody (2002) discussed accuracy classifications below 85%, contemplating a wide range in the accuracy with which individual classes were classified.

Water Practice & Technology Vol 15 No 3
doi: 10.2166/wpt.2020.049

The proportions of areas associated with LULC classes of classified maps in the Urama Basin from 1986 to 2017 show that the order of class occurrence prevalence is: a) vegetation (50–85%), b) agriculture (15–20%), c) rural areas (5–10%), d) bare soil (5–10%), e) waterbodies (5%), f) clouds (1–10%) and g) shadows (<1%). Comparing this method's results with those of the PCs method demonstrates that the pattern found in the spectral band co-variances in the optical infrared region (OIR) matches the spectral profile corresponding to vegetation or agricultural areas.

The post-classification method results using the change detection matrix corresponding to the recoded LULC classification maps, based on reflectance images in the basin from 1986 to 2017, are shown in Table 7. The total pixel area is 818,707 (736.84 km^2). The no change areas were: C1: 294,983 pixels (265 km^2, 36%), C2: 8 pixels (0.0072 km^2, 0.00097%), C3: 44,141 pixels (39.72 km^2, 5.39%), C4: 4,328 pixels (4 km^2, 0.54%), C5: 6,196 pixels (5.57 km^2, 0.75%). The LULC changes from C1 (vegetation) from 1986 to 2017 were: 93,940 pixels to agriculture (84.85 km^2), 36,030 to rural areas (32.42 km^2), and 52,559 to bare soil (47.3 km^2). In general, the bi-temporal change area varies between 36.89 and 57.28%; the no change area between 42.71 and 63.1%; and the change area average is C: 46.43% and NC: 53.55%.

Table 7 | Post-classification method results using change detection matrix corresponding to the LULC recoded classification maps based on reflectance images in the Urama Basin, 1986–2017

		2017 Classified Map							Total
		LULC class							(Pixels)
Year	LULC classes	1	2	3	4	5	6	7	
1986 Classified Map	1	**294,983**	1,413	93,940	36,030	52,559	530	2,146	
	2	1,938	**8**	1,373	832	1,554	31	32	
	3	107,758	663	**44,141**	16,747	23,910	171	969	
	4	52,256	135	19,667	**4,328**	10,620	131	403	
	5	21,855	149	10,490	3,455	**6,196**	70	193	
	6	1,815	0	743	188	438	**22**	8	
	7	2,401	4	614	387	396	10	**5**	
	Total	**483,006**	**2,372**	**170,968**	**61,967**	**95,673**	**965**	**3,756**	**818,707**
Change (Pixels)		**188,023**	**2,364**	**126,827**	**57,639**	**89,477**	**943**	**3,751**	**469,024**
No change (Pixels)		**294,983**	**8**	**44,141**	**4,328**	**6,196**	**22**	**5**	**349,683**

For example, the post-classification results using LULC recoded maps in 2000 and 2016 are shown in Figure 4. The year-by-year issues are as follows.

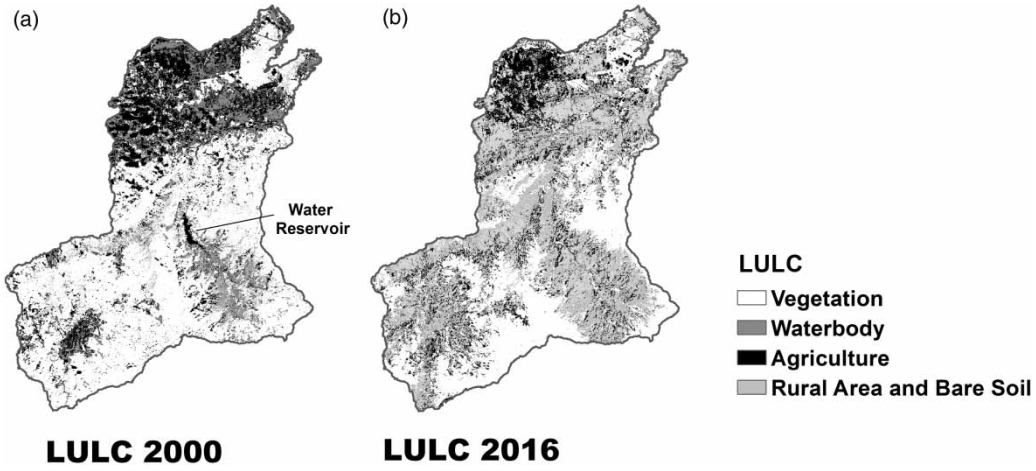

Figure 4 | Post-classification comparison method results from the Urama Basin from 1986 to 2017. (a) LULC in 2000 and (b) LULC in 2016.

Water Practice & Technology Vol 15 No 3
doi: 10.2166/wpt.2020.049

1986: most of the area is covered by vegetation, the reservoir near the middle is relatively new, there are agricultural areas in some high and low zones, with bare soil in an upper sub-basin and around the drainage network, connecting the reservoir with the Caribbean in the north of the basin.

1991: most of the area is covered by vegetation and, to a lesser extent, reservoirs and bare soil.

2000: the reservoir's supply zone is now protected, a rural use, as the agricultural area has expanded and there is bare soil in the lower part of the basin in wetland 1, close to the Caribbean.

2008: the water supply rural area and the agricultural area within wetland 1 have expanded.

2015: the area of bare soil in the reservoir's water supply protection zone has increased, with a decrease in the extent of the occupied area by the water reservoir, bare soil with agricultural use in the lower part of the basin (wetland 1).

2016: the extent of bare soil in the reservoir's resource protection zone, and in wetland 2 (near the middle of the basin) and wetland 1 (close to the Caribbean) has increased.

2017**:** the extent of the agricultural areas, and of bare soil throughout the basin, including areas around the two wetlands has increased.

The difference results from the LULC are presented in order of importance. Vegetation cover tends to increase by between about 5 and 25%, it is the most sensitive of the classes to change. Agricultural use decreased to a range of 5–15%. Rural use showed an annual increase between 2 and 5%. The only other significant variation was a decrease of 10% in degraded soil between 2000 and 2016, followed by an increase of less than 5% between 2016 and 2017.

CONCLUSIONS

For the tropical wetland studied, the NIR reflectance difference can be used to estimate LULC vegetation, agricultural use, and bare soil changes where reflectance is reasonably high. PC1, which includes the greatest reflectance variance in the satellite image n spectral bands, was the best option in the principal component difference method. It enabled the detection of changes in five LULC classes: waterbodies, rural areas, vegetation, agricultural use and bare soil. The post-classification method enables validation of classes where change/no change were detected using pre-classification methods.

The combination of methods described enables higher levels of accuracy in the LULC change predictions of the PC method in scenarios where one class is predominant, one of the characteristics of tropical wetlands. The Urama Basin scene has extensive vegetation cover. PC1 encompasses between 80 and 90% of the reflectance variance detected by Landsat sensors and was recorded in seven spectral bands. The eigenvalue vector results from the reflectance image dataset for the time period confirmed this. This is a significant difference from the reflectance differencing method, where reflectance corresponds to a specific spectral band, which is restrictive for detecting LULC change. The post-classification method has limitations because the supervised classification results depend on producer/user accuracy in classifying specific LULC classes.

Land-use and land-cover change dynamics will enable proposal of a management model for the Urama Basin wetland, identifying vegetation, waterbodies, agricultural use and bare soil as dynamic factors, to guide land management unit planning.

REFERENCES

ASF DAAC 2015 *ALOS PALSAR_Radiometric_Terrain_Corrected_low_res; Includes Material © JAXA/METI 2007*. Accessed through ASF DAAC. Available from: https://asf.alaska.edu 11 November 2015. doi:10.5067/JBYK3J6HFSVF.

Dahdouh-Guebas, F. 2002 The use of remote sensing and GIS in the sustainable management of tropical coastal ecosystems. *Environment, Development and Sustainability* **4**(2), 93–112. https://doi.org/10.1023/A:1020887204285.

Water Practice & Technology Vol 15 No 3
doi: 10.2166/wpt.2020.049

Foody, G. M. 2002 Status of land cover classification accuracy assessment. *Remote Sensing of Environment* **80**(1), 185–201. https://doi.org/10.1016/S0034-4257(01)00295-4.

Han, L. & Rundquist, D. C. 1997 Comparison of NIR/RED ratio and first derivative of reflectance in estimating algae chlorophyll concentration: a case study in a turbid reservoir. *Remote Sensing of Environment* **62**, 253–261. https://doi.org/10.1016/S0034-4257(97)00106-5.

Hayes, D. J. & Sader, S. A. 2001 Comparison of change detection techniques for monitoring tropical forest clearing and vegetation regrowth in a time series. In: *Photogrammetric Engineering & Remote Sensing*, Vol. 67. No. 9. pp. 1067–1075. Available from: https://www.asprs.org/wp-content/uploads/pers/2001journal/september/2001_sept_1067-1075.pdf.

Hussain, M., Chen, D., Cheng, A., Wei, H. & Stanley, D. 2013 Change detection from remotely sensed images: from pixel-based to object-based approaches. *ISPRS Journal of Photogrammetry and Remote Sensing* **80**, 91–106. Available from: https://www.journals.elsevier.com/isprs-journal-of-photogrammetry-and-remote-sensing/ (accessed 26 January 2018).

Ingebritsen, S. E. & Lyon, R. J. P. 1985 Principal component analysis of multitemporal image pairs. *International Journal of Remote Sensing* **6**(5), 687–696. https://doi.org/10.1080/01431168508948491.

Jensen, J. R. 2009 *Remote Sensing of the Environment: An Earth Resource Perspective*, 2nd edn. Pearson Education India, New Delhi, p. 613.

Kuria, D., Menz, G., Misana, S., Mwita, E., Thamm, H., Alvarez, M., Mogha, N., Becker, M. & Oyieke, H. 2014 Seasonal vegetation changes in the Malinda wetland using bi-temporal, multi-sensor, very high resolution remote sensing data sets. *Advances in Remote Sensing* **3**, 33–48. doi:10.4236/ars.2014.31004.

Lodhi, M. A., Rundquist, D. C., Han, L. & Juzila, M. S. 1997 The potential of remote sensing of loess soils suspended in surface waters. *Journal of the American Water Resources Association* **33**(1), 111–127. https://doi.org/10.1111/j.1752-1688.1997.tb04087.x.

Marquez, A., Guevara, E. & Rey, D. 2018a Assessment of land use and land cover change detection using eleven techniques of satellite remote sensing in the Pao River Basin, Venezuela. *Journal of Remote Sensing GIS & Technology* **4**(2), 1–70. Available from: http://matjournals.in/index.php/JORSGT/article/view/2764/ (accessed 8 August 2018).

Marquez, A. M., Guevara, E. & Rey, D. 2018b Analysis of methods to detect changes in coverage from water reservoirs of the Pao River Basin, Venezuela. *Journal of Remote Sensing GIS & Technology* **4**(2). Available from: http://matjournals.in/index.php/JORSGT/article/view/2734/ (accessed 8 August 2018).

Marquez, A. M., Guevara, E. & Rey, D. 2019 Hybrid model for forecasting of changes in land use and land cover using satellite techniques. *IEEE Journal of Selected Topics in Applied Earth Observations and Remote Sensing* **12**(1), 252–273. doi:10.1109/JSTARS.2018.2885612.

Munyati, C. 2000 Wetland change detection on the Kafue Flats, Zambia, by classification of a multitemporal remote sensing image dataset. *International Journal of Remote Sensing* **21**(9), 1787–1806. doi:10.1080/014311600209742.

Mwita, J. E. 2016 Monitoring restoration of the eastern Usangu wetland by assessment of land use and cover changes. *Advances in Remote Sensing* **5**, 145–156. doi:10.4236/ars.2016.52012.

Nikhil Raj, P. P. & Azeez, P. A. 2010 Land use and land cover changes in a tropical river basin: a case from Bharathapuzha River Basin, Southern India. *Journal of Geographic Information System* **2**(4), 185–193. doi:10.4236/jgis.2010.24026.

Petroquímica de Venezuela, S. A (PEQUIVEN). 2014 *Proyecto Desvío de la Troncal 3 con conexión a la Autopista Centro Occidental. Estudio Hidrológico. (Trunk 3 Deviation Project connected to the Central Western Highway. Hydrological Study)*. Complejo Petroquímico Morón, Venezuela, CA, G.F.M. Ingeniería.

Plant, N. G., Smith, K. E., Passeri, D. L., Smith, C. G. & Bernier, J. C. 2018 *Barrier-island and Estuarine-Wetland Physical-Change Assessment After Hurricane Sandy*. US Department of the Interior, US Geological Survey. Available from: https://pubs.usgs.gov/of/2017/1157/ofr20171157.pdf.

Saha, A., Tomar, S. & Kumari, M. 2017 Land use and land cover change monitoring of Surajpur Wetland, Uttar Pradesh: using GIS and remote sensing techniques. In *ESRI India User Conference*. Vol. 17, p. 1–8. Available from: https://www.academia.edu/32723777/Land_Use_and_Land_Cover_change_monitoring_of_Surajpur_Wetland_Uttar_Pradesh_using_GIS_and_Remote_Sensing_Techniques (accessed 5 December 2019).

Singh, A. 1989 Review article digital change detection techniques using remotely-sensed data. *International Journal of Remote Sensing* **10**(6), 989–1003. Retrieved February 02, 2018 from http://dx.doi.org/10.1080/01431168908903939/.

Sinha, P. & Kumar, L. 2013 Independent two-step thresholding of binary images in inter-annual land cover change/no-change identification. *ISPRS Journal of Photogrammetry and Remote Sensing* **81**, 31–43. https://doi.org/10.1016/j.isprsjprs.2013.03.010.

Spruce, J., Bolten, J., Mohammed, I. N., Srinivasan, R. & Lakshmi, V. 2020 Mapping land use land cover change in the Lower Mekong Basin from 1997 to 2010. *Frontiers in Environmental Science* **8**, 21. doi:10.3389/fenvs.2020.00021.

Trodd, N. M. 1995 Proceedings RSS95: remote sensing in action. In: *Uncertainty in Land Cover Mapping for Modelling Land Cover Change*. pp. 1138–1145.

U.S. Geological Survey 2017 *Landsat 8 OLI images. Accessed through USGS*. Available from: https://earthexplorer.usgs.gov/.